Available online at www.sciencedirect.com
ScienceDirect
Journal of the European Ceramic Society 29 (2009) 779–786
www.elsevier.com/locate/jeurceramsoc

Preparation, microstructure and mechanical properties of ZrB_2–ZrO_2 ceramics

Weijie Li *, Xinghong Zhang, Changqing Hong, Wenbo Han, Jiecai Han

Center for Composite Materials, Harbin Institute of Technology, Harbin 150001, PR China

Received 14 April 2008; received in revised form 2 June 2008; accepted 13 June 2008
Available online 21 August 2008

Abstract

ZrB_2–ZrO_2 ceramics with ZrO_2 content varied from 15 to 30 vol.% were prepared by hot pressing. The content of ZrO_2 was found to have an evident effect on the preparation, phase constitution, microstructure as well as the mechanical properties of ZrB_2–ZrO_2 ceramics. ZrB_2–30 vol.% ZrO_2 provided the optimal combination of dense microstructure (2.6 μm, as the average grain size) and excellent properties, including the flexural strength of 803 MPa, and the hardness of 22.7 GPa tested under 9.8 N. The highest t-ZrO_2 transformability of 35.2 vol.% during fracture for ZrB_2–30 vol.% ZrO_2 brought the best toughness of 6.5 MPa $m^{1/2}$ compared with any other ceramic. In addition, the dependence of toughness on the test method as well as the hardness on the indentation load was also investigated.

Keywords: Hot pressing; Mechanical properties; Phase transformation

1. Introduction

There is a growing interest in ZrB_2-based ceramics for their outstanding properties of high melting point, high electrical and thermal conductivities, chemical inertness and good oxidation resistance.[1] These properties make them attractive candidates for high temperature applications where corrosion-wear-oxidation resistance is demanded, such as ballistic armor, coating on cutting tools, electrical devices, nozzle and so on.[2–4] The fracture toughness of ZrB_2, with and without additives, is generally in the range of 3.5–4.5 MPa $m^{1/2}$.[1] For the most applications, however, such unsatisfactory value of toughness of ZrB_2 is still the obstacle to a wider range of use. The sinterability of ZrB_2 is limited due to its covalent bonding, high melting temperature and low self-diffusion coefficients of Zr and B. Many densification studies reported that hot pressing with high temperature and external pressure could provide the effective way to the full densification of ZrB_2.[5–7]

Zirconia ceramics have been investigated extensively for their excellent fracture toughness, strength, as well as other intrinsic physical and chemical properties including hardness, wear resistance, low coefficient of friction and thermal conductivity, and so on.[8] Concerning ZrO_2-based ceramics, the most attractive application was in the fields of general ceramics,[8–10] electrolytes or fuel cells,[11,12] as well as the films or thermal barrier coatings.[13,14] In particular, the most dramatic increase in the industrial applicability of ZrO_2 has been brought about by the discovery of the stress-induced phase transformation toughening from tetragonal to monoclinic phase.[8,15,16] Such phase transformation toughening mechanism was further investigated by so many researchers in the ZrO_2-based composites,[9,10,17–19] as well as the composites reinforced and toughened by ZrO_2.[20,21] The volume fraction of t-ZrO_2 available to transform to m-ZrO_2, called t-ZrO_2 transformability, was also evaluated to quantify the phase transformation.[9,17–19]

In this perspective, ZrO_2 was introduced to toughen ZrB_2-based ceramics. Hot pressing was applied to prepare ZrB_2–ZrO_2 ceramics with a content range of ZrO_2 from 15 to 30 vol.%. The dependence of phase constitution, microstructure, as well as the mechanical properties of the hot-pressed ceramics on the content of ZrO_2 was analyzed.

2. Experimental procedure

2.1. Preparation

Commercially available raw materials were used to prepare the hot-pressed ceramics in this work. The ZrB_2 powder

* Corresponding author. Tel.: +86 451 86402382; fax: +86 451 86402382.
E-mail address: lwjhit@126.com (W. Li).

0955-2219/$ – see front matter © 2008 Elsevier Ltd. All rights reserved.
doi:10.1016/j.jeurceramsoc.2008.06.033

Table 1
Nomenclature for the developed ZrB_2–ZrO_2 ceramics

Constitution	Designation
ZrB_2–15 vol.%ZrO_2	ZB15Z
ZrB_2–20 vol.%ZrO_2	ZB20Z
ZrB_2–25 vol.%ZrO_2	ZB25Z
ZrB_2–30 vol.%ZrO_2	ZB30Z

(purity > 99.4%, with a trace of MgO, Al_2O_3 and CaO) with a mean size of 2 μm was supplied from the Northwest Institute for Non-Ferrous Metal Research, China. The ZrO_2 (1 μm, Fanmeiya Powders Co., Ltd, Jiangxi, China) used here were 3 mol.% Y_2O_3 partially stabilized zirconia prepared by co-precipitation method (purity > 99.6%, with a trace of Al_2O_3 and SiO_2). Four kinds of ceramics were investigated, as listed in Table 1. The powder mixtures were ball-milled for 8 h in a polyethylene bottle using ZrO_2 balls and ethanol as the grinding media. After mixing, the slurry was dried in a rotary evaporator and screened. Milled powders were hot pressed at 1850 °C for 60 min under a uniaxial load of 30 MPa in Ar atmosphere.

2.2. Characterization

Crystalline phases were identified by X-ray diffraction (XRD, Rigaku, Dmax-rb). According to the formula of Toraya et al.,[9] the volume fraction of the m-ZrO_2 (V_m) was calculated by measuring the intensities of (1 1 1) and (1 1 $\bar{1}$) reflections of the monoclinic phase and the (1 1 1) peak of the tetragonal phase:

$$V_m = \frac{1.311X_m}{1 + 0.311X_m} \quad (1)$$

$$X_m = \frac{I_m(1\,1\,1) + I_m(1\,1\,\bar{1})}{I_m(1\,1\,1) + I_m(1\,1\,\bar{1}) + I_t(1\,1\,1)} \quad (2)$$

where X_m denoted the integrated intensity ratio, I_m and I_t were the peak intensities of the m-ZrO_2 and t-ZrO_2, respectively. The final density was measured by the Archimede's method, while the relative density was estimated by the rule of mixture. The microstructural features of the ceramics were observed by scanning electron microscopy (SEM, FEI Sirion, Holland) with simultaneous chemical analysis by energy dispersive spectroscopy (EDS, EDAX Inc.). The grain size of samples was determined by the line-intercept method from the SEM micrograph.[22] Transmission electron microscopy (TEM, JEM-2010) was applied to evaluate the interfaces in the ceramics.

Flexural strength (σ) was tested in three-point bending on 3 mm × 4 mm × 36 mm bars, using a 30 mm span and a crosshead speed of 0.5 mm min^{-1}. Each specimen was ground and polished with diamond slurries down to a 1 μm finish. The edges of all the specimens were chamfered to minimize the effect of stress concentration due to machining flaws. Microhardness (Hv) was measured by Vickers' indentation under three loads, i.e., 9.8, 29.4, and 49 N, applied for 10 s on the polished sections. Fracture toughness (K_{IC}) was evaluated by a single-edge notched beam (SENB) test with a 16 mm span and a crosshead speed of 0.05 mm min^{-1} using 2 mm by 4 mm × 22 mm bars, on the same jig used for the flexural strength. A minimum number of five specimens were tested for each experimental condition. It is noted that the toughness of ceramics is dependent on the test techniques. Short crack techniques involved measurement of crack lengths (radial/median) around hardness indentations by means of various models,[23,24] which was also applied to determine the toughness of present ZrB_2–ZrO_2 ceramics.

3. Results and discussion

3.1. Densification

The densification curves of ZB20Z and ZB30Z ceramics collected during hot pressing are plotted in Fig. 1(a) as the function of time, along with the temperature profile. The overall duration of the thermal treatment was about 210 min. ZB30Z started to shrink at about 1740 °C. After thermal treatment for 180 min, the relative density reached 98.9%. It was noted that ZB20Z needed to be treated for about 190 min to obtain the maximum densification. Apparently, higher content of ZrO_2 is beneficial for the densification of ZrB_2–ZrO_2 ceramics.

The relative density of four ceramics is presented in Fig. 1(b). With increase in ZrO_2 content, the densification of hot-pressed ceramics shows evident enhancement from 94.3% for ZB15Z to 98.9% for ZB30Z. More amounts of ZrO_2 bring beneficial effect on the densification of ZrB_2–ZrO_2 ceramics, which is attributed

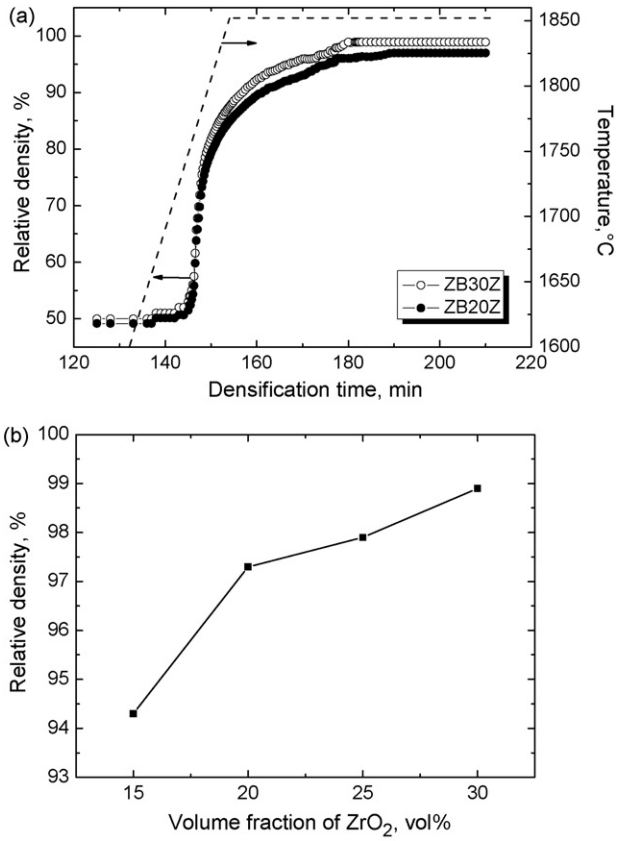

Fig. 1. Densification curves of hot-pressed ZB20Z and ZB30Z (a), and the plot of relative density (%) of hot-pressed ceramics with ZrO_2 content increased from 15 to 30 vol.% (b).

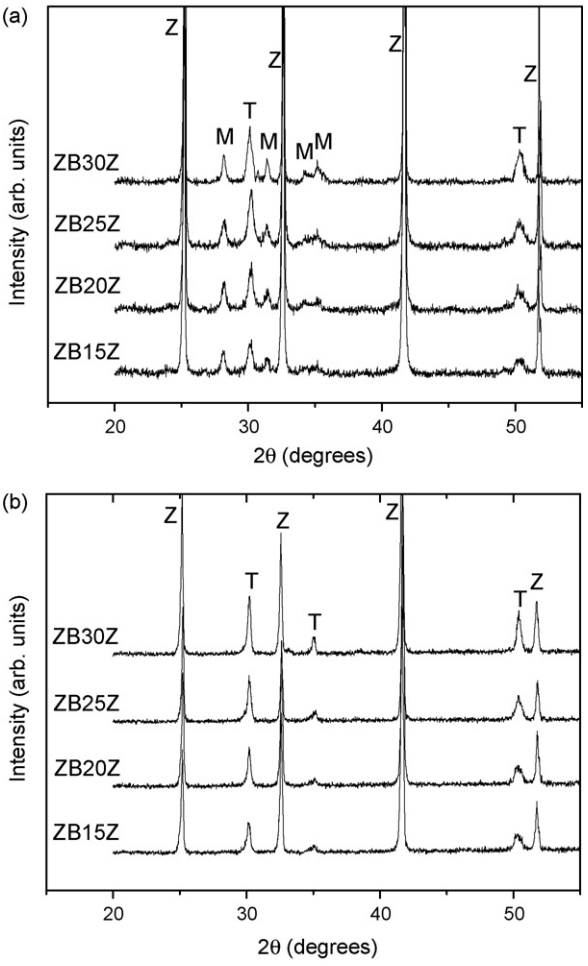

Fig. 2. XRD spectra obtained from the initial powder (a), and the polished surfaces (b) of hot-pressed ceramics, where Z, M and T denote the diffraction peaks of ZrB_2, m-ZrO_2 and t-ZrO_2, respectively.

to the contribution of ZrO_2, as the second reinforcing phase with smaller grain size.[20,21]

3.2. XRD analysis

The X-ray diffraction patterns in the 2θ range from 20° to 55° of the initial powder as well as the polished surfaces of hot-pressed ZrB_2–ZrO_2 ceramics are shown in Fig. 2. Apparently, the phase analysis indicates the predominant phases for the initial mixed powders of present ceramics are ZrB_2, t-ZrO_2 and m-ZrO_2 (Fig. 2(a)). When the volume fraction of ZrO_2 was increased from 15 to 30 vol.%, the intensity of diffraction peak of t-ZrO_2 as well as m-ZrO_2 gets stronger. However, too much of m-ZrO_2 phase has not been detected in the polished surface of ceramics. It is mainly ascribed to the phase transformation from m-ZrO_2 to t-ZrO_2 during hot pressing as reported.[17–19]

According to formula (1) and (2), the calculation results of the amount (vol.%) of m-ZrO_2 in the polished and fracture surfaces are listed in Table 2. Decrease in the volume fraction of m-ZrO_2 can be found on the polished surfaces with increased content of ZrO_2. More amounts of t-ZrO_2 retained after hot pressing in the ceramic with higher content of ZrO_2, which provided the probability that transformability from t-ZrO_2 to m-ZrO_2 during fracture would become considerable.[25,26] As shown in Table 2, more amounts of t-ZrO_2 were available to transform to m-ZrO_2 during fracture, which can be even up to 35.2 vol.% for ceramic ZB30Z.

3.3. Microstructure

Fig. 3 shows the polished-etched surfaces of the hot-pressed ceramics. Together with the fracture surface of ZB20Z in Fig. 4, EDS patterns reveal that the microstructure is characterized by the presence of coarser and elongated ZrB_2 matrix, as well as relatively finer and equiaxed ZrO_2 grains. Some small pores are distinguished in ZB15Z. With increase in the content of ZrO_2, denser microstructure was obtained as shown in Fig. 3(b)–(d). Moreover, the fracture surface in Fig. 4 indicates that ZrB_2 grains present fracture predominantly with transgranular mode, and ZrO_2 grains, dispersed among ZrB_2 grain boundaries, are in the intergranular mode.

The resulting average grain size of the hot-pressed ceramics is graphically depicted in Fig. 5. The average grain size of the ceramics decreases from 4.7 μm for ZB15Z to 2.6 μm for ZB30Z. This variation in grain size can be also observed in the polished surface of ceramics in Fig. 3. The introduction of smaller second phase, ZrO_2, effectively restrained the growth of grains during hot pressing, which became more significant with the higher content of ZrO_2. The restriction in grain growth could further improve the densification,[27] as described in Fig. 1.

Fig. 6 shows the bright field TEM micrograph of the interface between grains of ZrB_2 and ZrO_2 in ZB30Z. EDS pattern and the selected area electron diffraction (SAED) both reveal the central grain is tetragonal ZrO_2 with $c/a \approx 1.43$ as the lattice parameter ratio. Surrounding grains were confirmed as ZrB_2 with $c/a \approx 1.11$. A limited content of O–Mg–Al–Zr–Ca secondary phase, located at the triple-point boundaries of grains

Table 2
XRD quantification of the amount (vol.%) of m-ZrO_2 presented in the polished and fracture surfaces, and t-ZrO_2 transformability during fracture of the hot-pressed ZrB_2–ZrO_2 ceramics

Samples	vol.% m-ZrO_2 (polished surface)	vol.% m-ZrO_2 (fracture surface)	vol.% t-ZrO_2 transformability = (vol.% m-ZrO_2 in fracture surface − vol.% m-ZrO_2 in polished surface)
ZB15Z	36.2	43.1	6.9
ZB20Z	29.1	47.5	18.4
ZB25Z	26.4	43.4	17.0
ZB30Z	26.2	61.4	35.2

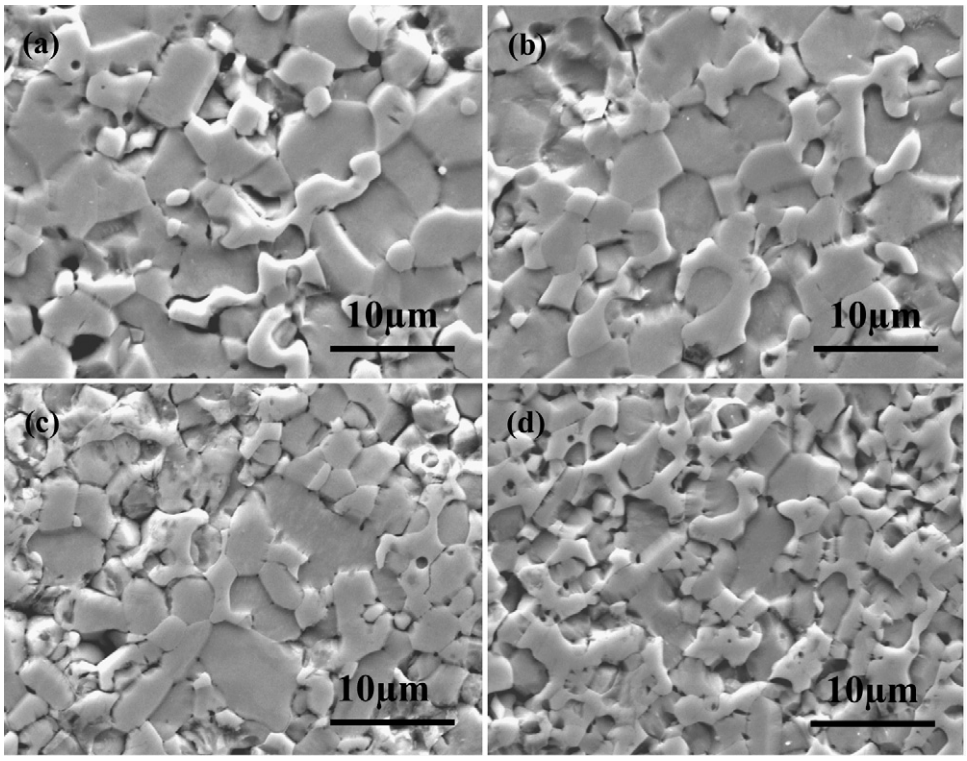

Fig. 3. SEM images of polished-etched surfaces of hot-pressed ZrB_2–ZrO_2 ceramics: ZB15Z (a), ZB20Z (b), ZB25Z (c), and ZB30Z (d).

of ZrB_2 and ZrO_2, was detected. SAED further indicates that the grain boundary phase is uncrystallized. Such glass phase was presumably related to the impurities in the initial powder of ZrB_2, which would be reacted to produce some oxides. During hot pressing, the low-eutectic-point oxides phase could enhance mass transfer, accelerate densification and lead to a high relative density.[28] Stacking faults, denoted by the small triangles, are detected between the grains of ZrB_2. Such defects

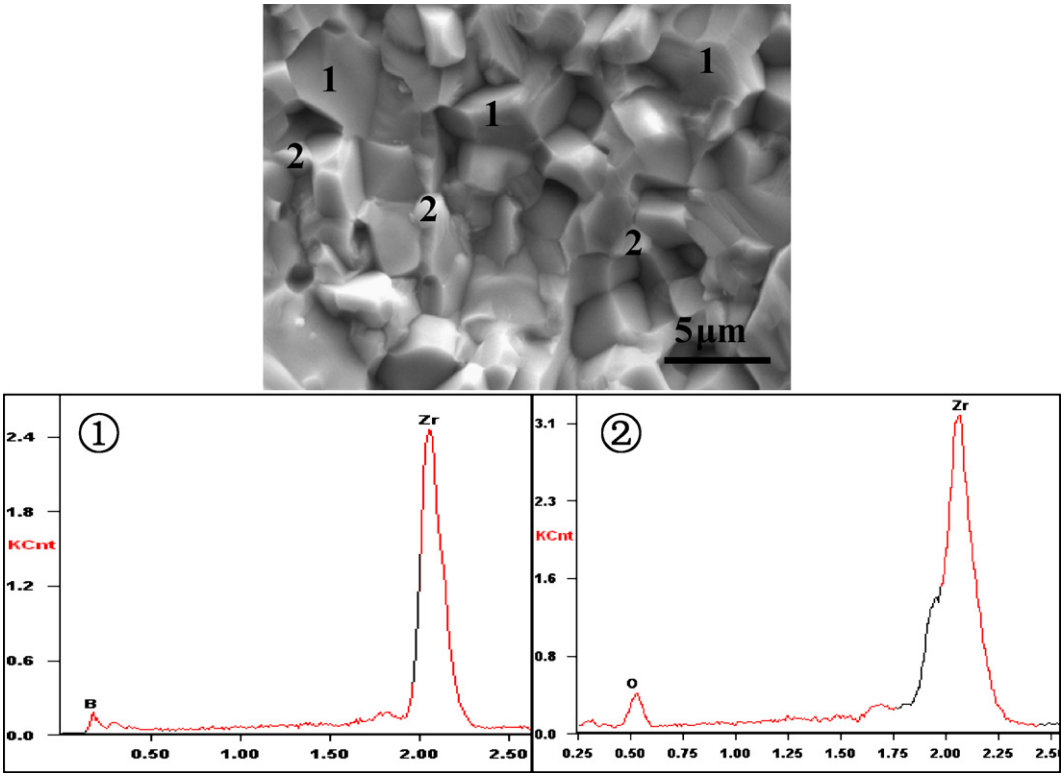

Fig. 4. Fracture surface of ZB20Z, EDS patterns show that bigger and coarser grains are ZrB_2, finer and equiaxed grains are ZrO_2.

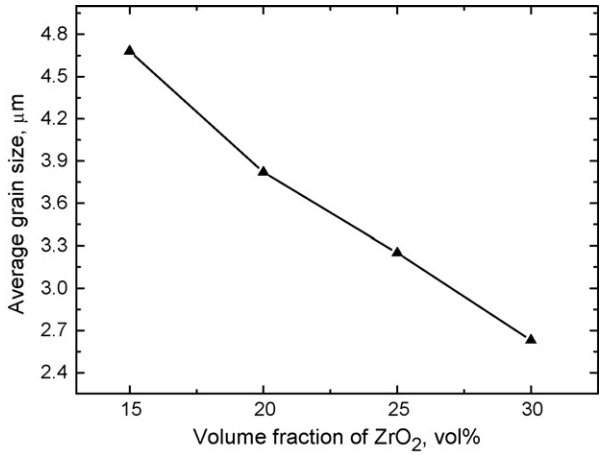

Fig. 5. Plot of the average grain size of hot-pressed ceramics with ZrO_2 content increased from 15 to 30 vol.%.

were induced by the misfit of atoms on the boundary, which is generally associated with the stress threshold.[29,30]

3.4. Mechanical properties

3.4.1. Flexural strength

The flexural strength of four ceramics, as shown in Fig. 7, presents improvement with increase in the content of ZrO_2. The strength is only 667 MPa for ZB15Z, however, ceramic ZB30Z exhibits the best, i.e., 803 MPa, which is partially ascribed to the denser microstructure as shown in Fig. 4. The finer grains are further responsible for the improved strength, according to the Hall–Petch relationship.[31]

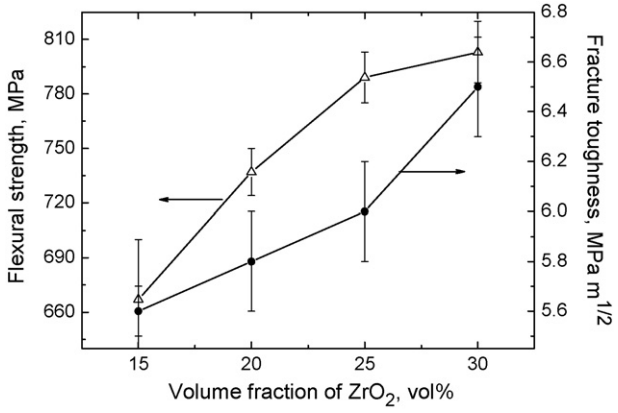

Fig. 7. Plots of flexural strength and fracture toughness (by SENB) of hot-pressed ZrB_2–ZrO_2 ceramics.

3.4.2. Toughness

As far as the fracture toughness tested by SENB is concerning (see Fig. 7), the increased content of ZrO_2 plays an active role in toughening the hot-pressed ceramics. With the content of ZrO_2 varied from 15 to 30 vol.%, the fracture toughness is numerically advanced from 5.6 to 6.5 MPa m$^{1/2}$. For the ceramics toughened by zirconia, the toughening mechanism is dominantly composed of two aspects,[21,32] i.e., crack deflection toughening induced by the second reinforcing phase, and stress-induced phase transformation toughening. In the case of crack deflection toughening, ZrO_2 grains, as the second reinforcing phase, hinder the crack growing or propagating (see Fig. 8). Consequent degradation in system energy leads to the enhancement in toughness.

According to the phase transformation toughening of ZrO_2, more amounts of t-ZrO_2 available transforming to m-ZrO_2

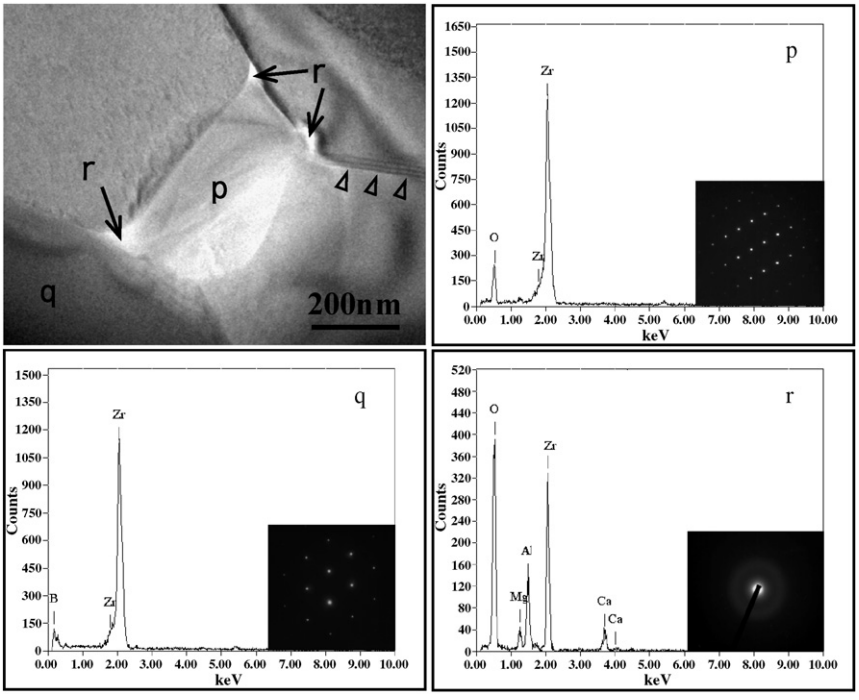

Fig. 6. Bright field TEM micrograph of grain interfaces obtained in ZB30Z.

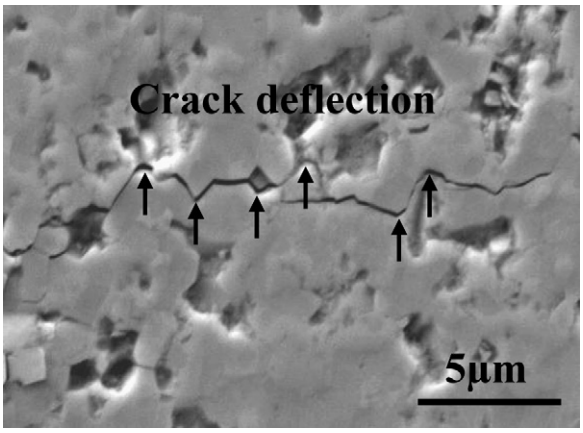

Fig. 8. SEM image of microcrack from Vickers' indentation on the polished surface of ZB25Z.

implies that greater progress was achieved to toughen the ceramics. As presented in Table 2, only 6.9 vol.% fraction of t-ZrO_2 was involved in the transformation for ZB15Z. Combined with the contribution of crack deflection, unsatisfactory toughness of 5.6 MPa $m^{1/2}$ was obtained for ZB15Z. When the content of ZrO_2 was varied from 20 to 25 vol.% the fraction of t-ZrO_2 transformability did not show evident difference. A small range from 5.8 to 6.0 MPa $m^{1/2}$ of toughness was provided for ZB20Z and ZB25Z. It is noted that ZB30Z exhibits a toughness of 6.5 MPa $m^{1/2}$. Such enhancement in toughness was interpreted primarily with the considerable t-ZrO_2 transformability, which was increased by ~100% from 17.0 vol.% for ZB25Z to 35.2 vol.% for ZB30Z. Further, 30 vol.% fraction of ZrO_2 reinforced ZrB_2 improved the toughening contribution from crack deflection. Both of the toughening from phase transformation and crack deflection resulted in the great enhancement in toughness of ZB30Z.

In order to further investigate the toughness of the present ceramics, the short crack technique was also applied. Fig. 9(a) gives a representative SEM image of Vickers' indentation from the polished surface of ZB20Z, which indicates the presence of radial cracks predominantly emanating from the indent corners. Corresponding schematic representation of a Vickers' indent is shown in Fig. 9(b), from which the relevant indentation data,

Table 3
Indentation data under load $P = 49$ N, i.e., average indent diagonal length ($2a$) and total crack length ($2c$), as well as the fracture toughness values for the hot-pressed ZrB_2–ZrO_2 ceramics

Samples	Indent diagonal, $2a$ (μm)	Crack length, $2c$ (μm)	l/a	Indentation toughness (MPa $m^{1/2}$)
ZB15Z	72.31	173.38	1.40	6.3 ± 0.3
ZB20Z	74.72	157.36	1.11	6.7 ± 0.2
ZB25Z	71.37	142.37	0.99	7.2 ± 0.3
ZB30Z	65.75	127.86	0.94	7.9 ± 0.4

i.e., the indent diagonal length ($2a$) and total crack length ($2c$), are provided in Table 3. According to the range of 0.9–1.4 as the ratio of l/a listed in Table 3, Eq. (3) was chosen to calculate the indentation toughness with $\eta = 0.0089$.[23,24] The dimensionless quantity, η, is a constant for a given indenter geometry, provided the volume is conserved within the "plastic zone" (adjacent to the indentation).[17]

$$K_{IC} = \eta\left(\frac{E}{H}\right)^{2/5}\frac{P}{(al^{1/2})} \quad (3)$$

where E is the elastic modulus, H is the Vickers' hardness, P is the indent load, $2a$ is the average indent diagonal length, $2c$ is the crack length, and $l = c - a$.

The calculated toughness is shown in Table 3. The results show an obvious increment from 6.3 MPa $m^{1/2}$ for ZB15Z to 7.9 MPa $m^{1/2}$ for ZB30Z, which is similar to the variation of toughness presented in Fig. 7. Compared with the toughness in Fig. 7, Table 3 shows the enhancement for all ceramics, which is coincident with the reported progress.[33] Such difference was ascribed to the contribution of the phase transformation induced at the crack tip of the indentation.[17]

3.4.3. Hardness

The hardness was previously found to be affected by test temperature, load, and so on.[34–36] The dependence of hardness on the measuring load has been extensively investigated.[35,37] Fig. 10 shows the Vickers' hardness of hot-pressed ZrB_2–ZrO_2 ceramics measured under three loads, 9.8, 29.4 and 49 N. The hardness presents the enhancement with the increased content

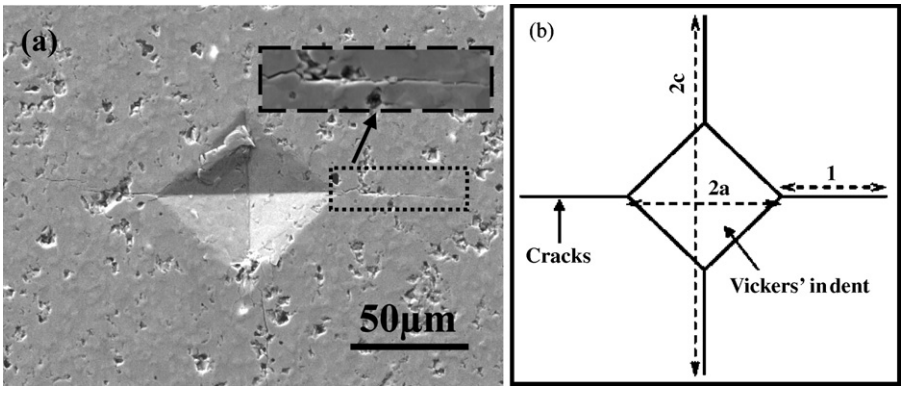

Fig. 9. SEM image of Vickers' indentation (taken at 49 N) on the polished surface of ceramic ZB20Z (a), and schematic representation of a Vickers' indent (b). The crack propagation from the indent edge has been shown in the inset of (a).

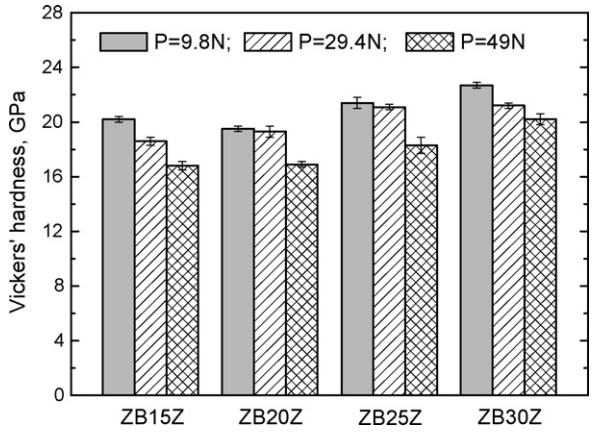

Fig. 10. Vickers' hardness of hot-pressed ZrB_2–ZrO_2 ceramics measured under the indentation loads of 9.8, 29.4 and 49 N.

of ZrO_2 due to the denser microstructure. In the case of ZB30Z, the hardness reaches 22.7 GPa measured under 9.8 N.

The load dependence of hardness is quite pronounced and the nature of decrease in hardness with increased load is of the same form in all ceramics, which is accordant with the previous work.[35,37] Such load dependence of hardness has been considered to originate from the fact that the measured diagonal of an indentation at a particular load is an apparent value, which remains associated with an uncertain amount of relaxation.[38] The extent of relaxation in an indentation diagonal occurs due to several possibility such as crack formation, dislocation activity and elastic recovery at the tip of the indentation.[38] This discussion further suggests that it is necessary to estimate hardness with methods not only the conventional procedure.

4. Conclusions

ZrB_2–ZrO_2 ceramics, with ZrO_2 content ranged from 15 to 30 vol.%, could be densified by hot pressing at 1850 °C under a pressure of 30 MPa. Higher content of ZrO_2 was beneficial to decrease the grain size, which was also advantageous for the strength. With increase in ZrO_2 content, decrease was presented for the volume fraction of m-ZrO_2 on the polished surface of ZrB_2–ZrO_2 ceramics. Evident increment in t-ZrO_2 transformability was found during fracture with increased content of ZrO_2, which caused the enhancement in fracture toughness. Further investigation of the toughness obtained by the indentation method showed the coincident variation with the one by SENB for ZrB_2–ZrO_2 ceramics. Vickers' hardness of the present ceramics was found to be dependent on the testing load. In short, ZrB_2–30 vol.%ZrO_2 ceramics provided optimal combination of microstructure and properties.

Acknowledgements

This work was supported by the National Natural Science Foundation of China (90505015, 50602010 and 50702016), the Research Fund for the Doctoral Program of Higher Education (20060213031) and the Program for New Century Excellent Talents in University. The authors are also grateful to the anonymous reviewers who provided many valuable comments for improving the presentation and quality of the final paper.

References

1. Fahrenholtz, W. G., Hilmas, G. E., Talmy, I. G. and Zaykoski, J. A., Refractory diborides of zirconium and hafnium. *J. Am. Ceram. Soc.*, 2007, **90**, 1347–1364.
2. Upadhya, K., Yang, J. M. and Hoffmann, W. P., Materials for ultrahigh temperature structural applications. *Am. Ceram. Soc. Bull.*, 1997, **76**, 51–56.
3. Opeka, M. M., Talmy, I. G. and Zaykoski, J. A., Mechanical, thermal, and oxidation properties of refractory hafnium and zirconium compounds. *J. Eur. Ceram. Soc.*, 1999, **19**, 2405–2414.
4. Schuldies, J. J. and Branch, T., Ultrasonic nde of ceramic components. *MCIC Report*, 1978, **3**, 429–448.
5. Meerson, G. A. and Gorbunov, A. F., Activated sintering of zirconium boride. *Inorg. Mater.*, 1968, **4**, 267–270.
6. Kalish, D., Clougherty, E. V. and Kreder, K., Strength, fracture mode and thermal stress resistance of HfB_2 and ZrB_2. *J. Am. Ceram. Soc.*, 1969, **52**, 30–36.
7. Melendez, J. J., Dominguez-Rodriguez, A., Monteverde, F., Melandri, C. and Portu, G., Characterisation and high temperature mechanical properties of zirconium boride-based materials. *J. Eur. Ceram. Soc.*, 2002, **22**, 2543–2549.
8. Hannink, R. H. J. and Kelly, P. M., Transformation toughening in zirconia-containing ceramics. *J. Am. Ceram. Soc.*, 2000, **83**, 461–487.
9. Toraya, H., Yoshimura, M. and Somiya, S., Calibration curve for quantitative analysis of the monoclinic-tetragonal ZrO_2 system by X-ray diffraction. *J. Am. Ceram. Soc.*, 1984, **67**, 119–121.
10. Li, J. F. and Watanabe, R., Fracture toughness of Al_2O_3-particle-dispersed Y_2O_3-partially stabilized zirconia. *J. Am. Ceram. Soc.*, 1995, **78**, 1079–1082.
11. Yang, C. C. T., Wei, W. C. J. and Roosen, A., Reaction kinetics and mechanics between $La_{0.65}Sr_{0.3}MnO_3$ and 8 mol% yttria-stabilized zirconia. *J. Am. Ceram. Soc.*, 2004, **87**, 1110–1116.
12. Knibbe, R., Drennan, J., Dicks, A. and Love, J., Effect of alumina additions on the anode electrolyte interface in solid oxide fuel cells. *J. Power Sources*, 2008, **179**, 511–519.
13. Laukaitis, G., Dudonis, J., Orliukas, A. F. and Milcius, D., Properties of YSZ thin films deposited by e-beam technique. *Solid State Sci.*, 2008, **179**, 182–187.
14. Jadhav, A. D., Padture, N. P., Jordan, E. H., Gell, M., Miranzo, P. and Fuller Jr., E. R., Low-thermal conductivity plasma-sprayed thermal barrier coatings with engineered microstructures. *Acta Mater.*, 2006, **54**, 3343–3349.
15. Garvie, R. C., Hannink, R. H. J. and Pascoe, R. T., Ceramic steel? *Nature (London)*, 1975, **258**, 703–704.
16. Porter, D. L. and Heuer, A. H., Mechanisms of toughening partially stabilized zirconia (PSZ). *J. Am. Ceram. Soc.*, 1977, **60**, 183–184.
17. Basu, B., Venkateswaran, T. and Kim, D., Microstructure and properties of spark plasma-sintered ZrO_2–ZrB_2 nanoceramic composites. *J. Am. Ceram. Soc.*, 2006, **89**, 2405–2412.
18. Basu, B., Vieugels, J. and Biest, O. V., Processing and mechanical properties of ZrO_2–TiB_2 composites. *J. Eur. Ceram. Soc.*, 2005, **25**, 3629–3637.
19. Chen, F. R., Ubic, F. J., Parkash, V. and Heuer, A. H., Stress-induced martensitic transformation and ferroelastic deformation adjacent microhardness indents tetragonal zirconia single crystals. *Acta Mater.*, 1998, **46**, 2151–2171.
20. Rapacz-Kmita, A., Slosarczyk, A. and Paszkiewicz, Z., Mechanical properties of HAp–ZrO_2 composites. *J. Eur. Ceram. Soc.*, 2006, **26**, 1481–1488.
21. Basu, B., Lee, J. H. and Kim, D. Y., Development of WC-ZrO_2 nanocomposites by spark plasma sintering. *J. Am. Ceram. Soc.*, 2004, **87**, 317–319.
22. Fullman, R. L., Measurement of particle sizes in opaque bodies. *Trans. AIME*, 1953, **197**, 447–452.
23. Anstis, G. R., Chantikul, P., Lawn, B. R. and Marshll, D. B., A critical evaluation of indentation techniques for measuring fracture toughness. *J. Am. Ceram. Soc.*, 1981, **64**, 553–557.

24. Palmqvist, S., Occurrence of crack formation during Vickers' indentation as a measure of the toughness of hardness materials. *Arch Eisenhuettenwes*, 1962, **33**, 629–633.
25. Jin, X. H., Gao, L., Kan, Y. M., Chen, Y. R. and Yuan, Q. M., Effects of Nb_2O_5 on the stability of t-ZrO_2 and the mechanical properties of ZTM. *Mater. Lett.*, 2002, **52**, 10–13.
26. Teng, L. D., Li, W. C. and Wang, F. M., Effect of Ti content on the martensitic transformation in zirconia for Ti–ZrO_2 composites. *J. Alloys Compd.*, 2001, **319**, 228–232.
27. Tadokoro, S. K. and Muccillo, E. N. S., Physical characteristics and sintering behavior of ultrafine zirconia–ceria powders. *J. Eur. Ceram. Soc.*, 2002, **22**, 1723–1728.
28. Hwang, S. S., Vasiliev, A. L. and Padture, N. P., Improved processing and oxidation-resistance of ZrB_2 ultra-high temperature ceramics containing SiC nanodispersoids. *Mater. Sci. Eng. A*, 2007, **464**, 216–224.
29. Liu, Y. C., Yang, G. C. and Zhou, Y. H., Phase competition in the undercooled hypoperitectic $Ti_{47}Al_{53}$ alloy. *Mater. Lett.*, 2002, **57**, 315–324.
30. Rae, C. M. F. and Reed, R. C., Primary creep in single crystal superalloys: origins, mechanisms and effects. *Acta Mater.*, 2007, **55**, 1067–1081.
31. Armstrong, R. W., The influence of polycrystal grain size on several mechanical properties of materials. *Metall. Trans.*, 1970, **65**, 1169–1171.
32. Bermejo, R., Pascual, J., Lube, T. and Danzer, R., Optimal strength and toughness of Al_2O_3–ZrO_2 laminates designed with external or internal compressive layers. *J. Eur. Ceram. Soc.*, 2008, **28**, 1575–1583.
33. Calderon-Moreno, J. M. and Popa, M., Fracture toughness anisotropy by indentation and SEVNB on tetragonal PZT polycrystals. *Mater. Sci. Eng. A*, 2001, **319–321**, 692–696.
34. Wolf, B., Bambauser, K. O. and Paufler, P., On the temperature dependence of the hardness of quasicrystals. *Mater. Sci. Eng. A*, 2001, **298**, 284–295.
35. Dutta, A. K., Narasaiah, N., Chattopadhyaya, A. B. and Ray, K. K., The load dependence of hardness in alumina–silver composites. *Ceram. Inter.*, 2001, **27**, 407–413.
36. Gong, J. H., Miao, H. Z. and Hu, B. J., Compositional dependence of hardness of (CeY)-TZP/Al_2O_3 composites. *Mater. Sci. Eng. A*, 2004, **372**, 207–212.
37. Guicciardi, S., Balbo, A., Sciti, D., Melandri, C. and Pezzotti, G., Nanoindentation characterization of SiC-based ceramics. *J. Eur. Ceram. Soc.*, 2007, **27**, 1399–1404.
38. Li, Z., Ghosh, A., Kobayashi, A. S. and Bradt, R. C., Indentation fracture toughness of sintered silicon carbide in Palmqvist crack regime. *J. Am. Ceram. Soc.*, 1989, **72**, 904–911.